HHS Public Access

Author manuscript

J Orthop Res. Author manuscript; available in PMC 2024 November 01.

Published in final edited form as:

J Orthop Res. 2023 November ; 41(11): 2384–2393. doi:10.1002/jor.25564.

Reduced Angiogenesis and Delayed Endochondral Ossification in CD163−/− Mice Highlights a Role of M2 Macrophages During Bone Fracture Repair

Youliang Ren[1,2], **Shiyang Zhang**[1,2], **Jason Weeks**[1,2], **Javier Rangel-Moreno**[1,3], **Bin He**[1,2], **Thomas Xue**[1,2], **Joshua Rainbolt**[1], **Yugo Morita**[1,2], **Ye Shu**[1,2], **Yuting Liu**[1,2], **Stephen L. Kates**[4], **Edward M. Schwarz**[1,2], **Chao Xie**[1,2,*]

[1]Center for Musculoskeletal Research, University of Rochester Medical Center, Rochester, NY, USA

[2]Department of Orthopaedics and Rehabilitation, University of Rochester Medical Center, Rochester, NY, USA

[3]Department of Medicine, University of Rochester Medical Center, Rochester, NY, USA

[4]Department of Orthopaedic Surgery, Virginia Commonwealth University, Richmond, VA, USA

Abstract

While recent studies showed that macrophages are critical for bone fracture healing, and lack of M2 macrophages have been implicated in models of delayed union, functional roles for specific M2 receptors have yet to be defined. Moreover, the M2 scavenger receptor CD163 has been identified as a target to inhibit sepsis following implant associated osteomyelitis, but potential adverse effects on bone healing during blockage therapy have yet to be explored. Thus, we investigated fracture healing in C57BL/6 vs. CD163−/− mice using a well-established closed, stabilized, mid-diaphyseal femur fracture model. While gross fracture healing in CD163−/− mice was similar to that of C57BL/6, plain radiographs revealed persistent fracture gaps in the mutant mice on day 14, which resolved by day 21. Consistently, 3D vascular micro-CT demonstrated delayed union on day 21, with reduced bone volume (74%, 61%, and 49%) and vasculature (40%, 40% and 18%) compared to C57BL/6 on days 10, 14, and 21 post-fracture respectively (p<0.01). Histology confirmed large amounts of persistent cartilage in CD163−/− vs. C57BL/6 fracture callus on day 7 and 10 that resolves over time, and immunohistochemistry demonstrated deficiencies in $CD206^+$ M2 macrophages. Torsion testing of the fractures confirmed the delayed early union in CD163−/− femurs, which display decreased yield torque on day 21, and a decrease rigidity with a commensurate increase in rotation at yield on day 28 (p<0.01). Collectively, these results demonstrate that CD163 is required for normal angiogenesis, callus formation, and bone remodeling during fracture healing, and raise potential concerns about CD163 blockade therapy.

*To whom correspondence should be addressed. chao_xie@urmc.rochester.edu.

Authors' contribution statement: All authors participated in the discussion, contributed to the writing, and have read and approved the final submitted manuscript.

Keywords

Fracture Healing; Angiogenesis; M2 Macrophages; CD163; Knockout Mice

Introduction

Although there have been major advances to treat fractures, 5 to 10% of patients fail to achieve satisfactory healing, which highlights the need for additional research to improve our understanding and clinical outcomes [1]. At the cellular and molecular level, fracture healing is a highly orchestrated biological process that can be characterized in three phases [2; 3]. While an extensive literature exists on the initial inflammatory and osteogenic phases of fracture healing, the osteoimmunology of cartilage and bone remodeling in the last phase has only been interrogated recently. This research confirmed that a wide array of inflammatory cells collaborate in fracture healing[3], including macrophages that are required for initiation and progression of early endochondral ossification[4], and osteoblastic differentiation[5].

It also confirmed that cellular heterogeneity exists, most notably “M1” pro-inflammatory macrophages that initiate angiogenesis and the osteogenic phase, and “M2” anti-inflammatory/reparative macrophages [6].

Preclinical functional studies have shown that depletion of macrophages negatively affects bone fracture healing [7; 8]. More specifically, M2 macrophages have been implicated in murine models of osteoporotic fracture healing [9–11], and high fluoride ingestion was shown to impair fracture healing by attenuating M2 macrophage differentiation [12]. Thus, modulating macrophage polarization for the enhancement of fracture healing has been recognized to be a therapeutic target, and the subject has been systemically reviewed[13]. Some of these M2 macrophage polarizing treatments, including: interleukin 4 and 13 (IL-4 & IL-13), vibration,[14] trehalose,[15] and nanoparticles magnetically delivered to the fracture site [16]. There have also been clinical studies that demonstrated M2 macrophages are closely associated with accelerated clavicle fracture healing in patients with traumatic brain injury [17]. Collectively, these studies demonstrate the critical role of M2 macrophages in endochondral ossification, and the importance of M1/M2 macrophage functional balance for efficient fracture healing. Thus, studies to identify specific M2 macrophage receptors for the regulation of the fracture healing are warranted.

In addition to elucidating the role of M2 macrophages in fracture healing, we are also interested in the specific function of the scavenger receptor CD163, which is expressed on monocytes and macrophages lineage cells exclusively[18]. CD163 knockout mouse studies demonstrated its functional role in the regulation of inflammatory cytokine expression in septic/endotoxin shock and collagen antibody-induced arthritis [19]. Although CD163−/− mice do not display any gross skeletal or immunological abnormalities, we found that CD163 is required for the generation of “Trojan horse” leukocytes and bacterial dissemination during the establishment of *Staphylococcus aureus* (*S. aureus*) implant-associated osteomyelitis in mice [20]. Specifically, we demonstrated that a multimolecular complex containing *S. aureus* protein A, antibodies against the iron surface determinant protein B (IsdB), IsdB

antigen, and the hemoglobin-haptoglobin (Hb-Hp) complex, mediates CD163-dependent bacterial internalization of macrophages in vitro. Additionally, CD163−/− mice are resistant to sepsis following *S. aureus* infection, as are wild-type (C57 BL/6) mice given anti-CD163-neutralizing antibodies [20]. While these genetic and biologic CD163 deficiencies did not exacerbate local infection, suggesting that CD163 blockade may be an effective therapy to prevent and treat sepsis, effects on bone healing were not investigated. Thus, we aimed to test the hypothesis that CD163 is not required for normal fracture healing in mice.

Materials and Methods

In vivo studies.

All *in vivo* experiments were performed according to IACUC approved protocols and utilized the murine closed, stabilized, mid-diaphyseal femur fracture model with 10-12 week-old female C57 BL/6 and CD163$^{-/-}$ (Cd163$^{tm1.1(KOMP)Vlcg}$) mice in a C57BL/6 background obtained from the Jackson Laboratory (Bar Harbor, ME, USA), as we have previously described [21]. Briefly, a stainless steel 25G spinal needle (BD, Franklin Lakes, NJ) was inserted into the intramedullary space of the femur, followed by three-point bending with an Einhorn device using a standardized force [22]. Longitudinal X-rays were obtained on days 0, 3. 5. 7. 10, 14, and 21 with a Faxitron cabinet x-ray system (Faxitron, Wheeling, IL, USA), and fractured femurs ($n \geq 10$) were harvested and processed for micro-CT, histological, and biomechanical analyses on days 14, 21, and 28 as previously described [23; 24].

MicroCT Imaging analyses:

Femurs were harvested at indicated times and scanned using a Viva microCT system (Scanco Medical, Bassersdorf, Switzerland) at a voxel size of 10.5 μm to image bone or vasculature. New bone formation and vascular volume were measured as previously described [25 26]. Briefly, a lead chromate-based contrast agent, Microfil, was used to perfuse the mice via the heart along with 4% paraformaldehyde. Samples were scanned before and after decalcification. Using proprietary software provided by Scanco, the periosteal external calluses were contoured and examined for bone volume and vascularization. To measure the vasculature, contour lines were drawn in the 2D slice images to exclude the cortical bone and the vessels in the surrounding tissues [27]. Histomorphometric analysis based on direct distance transform methods [28; 29] was subsequently performed on the 3D images to quantify parameters of vascular network morphology, including vasculature volume (Vasc.Vol.), vessel thickness (Vess.Th.), and vessel spacing (Vess.Sp).

Histology and Multicolor immunofluorescence:

All femurs were harvested at above indicated time points and processed for Alcian Blue Hematoxylin/ Orange G Stain and tartrate-resistant acid phosphatase (TRAP) staining in osteoclasts. At the mid-point of the femur on the sagittal cuts, five 5 μm tissue sections were obtained from three levels and mounted onto slides. Slides were deparaffinized, sequentially hydrated and placed in Acid-alcohol for 30 seconds. Slides were briefly drained on a paper towel and placed in Alcian Blue Hematoxylin for 25 minutes. Slides were then gently washed in distilled water (4 changes), differentiated in Acid-alcohol for 3 seconds and

gently rinsed gently in distilled water (3 changes). Slides were kept in 0.5% Ammonium water for 15 seconds, rinsed in distilled water (2 changes), placed in 95% EtOH for 1 minute and incubated in Eosin/ Orange G for 1 min 30 sec. Tissues were sequentially dehydrated with 95% EtOH (3 changes) and 100% EtOH (2 changes, 1 minute per change). Before mounting, slides were cleared with 3 changes of xylene and coverslipped. To perform TRAP staining, we took deparaffinized slides and placed them in a pre-warmed mix of TRAP staining solution. The slides were then incubated at 37°C for 30 minutes, followed by a counterstain with 0.08% Fast Green for 1.5 minutes. Finally, the slides were processed for mounting.

Immunofluorescent stain with CD206, iNOS, and F4/80 to detect M1 and M2 macrophages in bone fracture. Primary antibodies: Goat anti-CD206 (Cat# AF2535, RRID:AB_2063012, R&D Systems, Minneapolis, MN) at 1:100 dilution, Rabbit anti-iNOS at 1:100 dilution (Cat # NB300-605, RRID:AB_10002794, Novus Biologicals, Littleton, CO), and rat anti-mouse F4/80 at 1:50 dilution (clone Cl:A3-1, RRID:AB_323279, BioRad, Hercules, CA). Secondary antibodies: Alexa Fluor 568 donkey anti-goat IgG (A11057, RRID:AB 142581, Thermo Fisher Scientific, Waltham, MA), Alexa fluor 488 donkey anti-rabbit IgG (711-546-152, RRID:AB 2340619, Jackson ImmunoResearch Laboratories, Bar Harbor, ME) and Alexa fluor 647 donkey anti-rat IgG (712-606-153, RRID:AB_2340696, Jackson ImmunoResearch Laboratories). All secondary antibodies were used at 1: 200 dilution. Briefly, 5 μm formalin-fixed paraffin sections were incubated at 60°C overnight for deparaffinization. Tissue sections were quickly transferred to xylenes and gradually hydrated by transferring slides to absolute alcohol, 96% alcohol, 70% alcohol and water. Slides were immersed in 1X Dako antigen retrieval solution (S1699, Agilent, Santa Clara, CA), boiled for 30 minutes and cooled down for 10 minutes at room temperature (RT). Slides were rinsed several times in water and transferred to PBS. Non-specific binding was blocked with 5% normal donkey serum in PBS containing 0.1% Tween 20 and 0.1% Triton-X-100 for 30 minutes, at RT in a humid chamber. Primary antibodies were added to slides and incubated in a humid chamber at RT, overnight. Slides were quickly washed in PBS and fluorescently labeled secondary antibodies were incubated for 2 hours at RT in a humid chamber. Finally, slides were rinsed for 1 hour in PBS and mounted with Vectashield antifade mounting media with DAPI (H-1200, Vector Laboratories, Burlingame, CA). Pictures were taken with a Zeiss Axioplan 2 microscope and recorded with a Hamamatsu camera.

Biomechanical torsion testing.

Following removal of all soft tissues the unfixed fractured femurs were potted in polymethylmethacrylate, and the torsional biomechanical properties were determined using an EnduraTec TestBench system (200 N.mm torque cell; Bose Corporation, Minnetonka, MN) at a rate of 1°/s as previously described [24]. Ultimate torque, yield torque, torsional rigidity, and energy to failure at ultimate torque were determined for each specimen.

Statistical analysis:

Data are expressed as the mean ± standard error of the mean (SEM). Statistical significance between experimental groups was determined using one-way ANOVA and a Tukey's post-

hoc test (GraphPad Prism, San Diego, CA). A p value <0.05 was considered statistically significant.

Results

Radiographic evidence of delayed fracture healing in CD163−/− mice.

C57 BL/6 and CD163−/− mice underwent closed, stabilized, mid-diaphyseal femur fractures, and longitudinal X-rays were obtained on days 0, 3, 5, 7, 10, 14, and 21 post-fracture to assess 2D radiographic healing (Figure 1). The results showed evidence of a persistent fracture gap in the mutant mice on day 14, which resolved by day 21. To confirm this observation and investigate potential defects in angiogenesis, we performed vascular micro-CT analyses on femurs harvested on day 10, 14 or 21 post-fracture (Figure 2). Consistent with the plain radiographs, 3D renderings of femurs from the CD163−/− mice displayed an apparent delayed union on day 21, with gross decreases in fracture callus and vasculature (Fig. 2A). Quantitative analyses revealed that compared with C57 BL/6 fractures, the bone volume in CD163−/− fractures was reduced 74%, 61% ($p<0.01$), and 49% ($p<0.01$); and the vasculature was reduced to 40%, 40% (**$p<0.01$), and 18% (***$p<0.001$), on days 10, 14, and 21 post-fracture respectively.

Histologic evidence of delayed fracture healing and impaired accumulation of M2 macrophages in CD163$^{-/-}$ mice.

Demineralized histology to elucidate the vascular defects and delayed union and immunofluorescence for detecting INOS^{+}F4/80^{+} M1 and CD206^{+}F4/80^{+} M2 macrophages was performed on femurs on days 5, 7, 10, 14 and 21 post-fracture in CD163$^{-/-}$ and C57BL/6 mice (Figure 3). Visual assessment of the OG/AB-stained histology revealed large amounts of persistent Alcian blue stained cartilage in fracture callus of CD163$^{-/-}$ vs. C57BL/6, on days 7 and 10 (Fig. 3A). Visiopharm histomorphometry confirmed that fracture callus in CD163$^{-/-}$ mice had decreased bone with a commensurate increase in cartilage and undifferentiated mesenchymal tissue on day 10 and resolved over time (Fig. 3B). Interestingly, while CD206^{+}F4/80^{+} M2 macrophages were numerous in the fracture callus of C57BL/6 throughout the healing time course, CD206^{+}F4/80^{+} M2 macrophages were almost absent in the fracture callus from CD163$^{-/-}$ mice (Fig. 3A), suggesting CD163 deficiency altered the accumulation of M2 macrophages. Further TRAP-stained histology was performed using adjacent slides from ABH/OG and IF on day 14 and day 21 fractures and the results indicated that there were no differences in the osteoclasts surrounding the fracture callus between WT and CD163−/− fractures (Fig. 4).

Defective biomechanical fracture healing in CD163−/− mice.

To assess the functional significance of the radiographic and histological defects observed in CD163−/− fractured femurs, torsion testing was performed on C57 BL/6 and CD163−/− fractured femurs harvested on day 14, 21 or 28 post-fracture (Figure 5). Consistent with the delayed early union (Figs 1 and 2A), we found that CD163−/− femurs display decreased yield torque on day 21. Consistent with the persistent cartilage phenotype (Fig. 3A & B), we found that CD163−/− femurs displayed a decrease in torsional rigidity with a commensurate increase in rotation at yield at day 28.

Discussion

Given the unmet clinical need for 5-10% of fracture patients that experience delayed or non-unions [30], which often require extensive surgical interventions that are associated with a poor quality of life at great cost to our healthcare system [31], research efforts are warranted to improve our understanding of this complex biological process towards better interventions [32]. While opportunities exist to improve treatment options for the inflammatory [33] and osteogenic [34] phases of fracture healing, there are no standard of care treatments to enhance the remodeling phase of fracture healing largely due to our lack of knowledge. Thus, focused studies on cells whose primary function are tissue repair have been increasing, and have shed light on the important roles of M2 macrophages as both anti-inflammatory effector and anabolic cells [35].

Aging is among the dominant co-morbidities associated with fracture healing insufficiencies [36]. Although age-related defects in fracture healing are strongly associated with decreases in stem and progenitor cells [37], it is also known that aging shifts the M1:M2 ratio towards M1 in the elderly [38]. As this transition promotes a chronic pro-inflammatory scenario that interferes with effective healing [39], investigators proposed shifting the macrophage response towards M2 to enhance healing outcomes and minimize recuperation times [7]. The importance of macrophage subtypes in musculoskeletal disease and repair is also highlighted by recent article's focus on M1 [40; 41] and M2 [42–44] macrophages and their polarization is various connective tissues including tendon [45] and intervertebral disk [46].

While experimental methods to bias myelopoiesis towards M2 exist [47], our understanding of the functional receptors within this subset of regenerative macrophages remains limited. Currently, the receptors selectively expressed on M2 macrophages are largely considered to be phenotypic markers [48], rather than functional molecules that are actively involved in the reparative process. One exception is CD163, which is a scavenger receptor [18], and is known to be function on anti-inflammatory macrophages [49]. It's functions include clearance of cell-free hemoglobin and haptoglobin and anti-inflammatory cytokine-like activities [18]. Interestingly, it is known that brain tissue from multiple sclerosis patients contains an accumulation of $CD163^+$ macrophage/microglia cells in acute active lesions and at the rim of chronic active lesions. This suggests that CD163 might contribute to the resolution of inflammation [50]. Thus, we hypothesized that CD163 might function at the transition of the inflammatory to osteogenic phase of fracture healing. Although our histomorphometry studies identified a significant increase in the amount of undifferentiated mesenchyme tissue on day 7 in CD163−/− vs. C57 BL/6 fractures (Fig. 3B), this was the only difference we found between groups at this timepoint. In contrast, we observed several defects at the transition of the osteogenic to remodeling phase of fracture healing, which we conclude is where CD163 functions in this process.

Here we report that CD163−/− fracture callus has deficiencies in bone and vascular volume during remodeling on days 14 and 21 (Figure 2). Of particular note is that the vascular deficiencies are specific to angiogenesis as evidenced by the lack of small blood vessels (<0.15mm), while differences in larger vessels were not apparent on day 21 post-fracture (Fig. 2F). As we previously reported that teriparatide-induced bone formation is specifically

associated with small vessel angiogenesis [24; 51], and large vessel arteriogenesis leads to mast cell accumulation and fibrosis within bone defects [52; 53], this is consistent with CD163+ M2 macrophages playing a role in vascularizing the soft fracture callus during the osteogenic phase. This conclusion is also supported by the persistent cartilage and undifferentiated mesenchyme on day 10 in CD163−/− fracture callus (Fig. 3), which manifests as radiographic non-union on day 14 (Fig. 1). It is also consistent with the biomechanical deficiencies of delayed early union, in which CD163−/− fracture femurs display decreased yield torque on day 21, and a decreased rigidity with a commensurate increase in rotation at yield at day 28 (Fig. 5).

Perhaps our most interesting and hypothesis generating finding is the lack of macrophages in CD163$^{-/-}$ fracture callus throughout healing (Fig. 3). While the loss of CD206+ cells was predicted by the absence of a functional M2 receptor, the absence of F4/80+ cells, which includes all tissue macrophages, remains unexplained and an important topic for future research. As the first assessment of the role of CD163 in fracture healing, this study also contains several notable limitations that should be addressed in subsequent work. These include a comprehensive assessment of the macrophage populations via flow cytometry and single-cell RNAseq. Additionally, since global knockout mice were used, our findings cannot differentiate phenotypes from loss of CD163 during fracture healing versus developmental cell defects. Thus, studies with a conditional-inducible CD163 gene deletion model, or immunodepletion with anti-CD163 antibodies could be helpful in sorting this out. Additionally, we only evaluated adult female mice. Thus, future studies focused on addressing a potential role of CD163 and M2 macrophages in aged, osteoporotic, and diabetic fracture healing are warranted. Nevertheless, here we demonstrate a functional role for this important M2 marker in bone repair, which warrants further research to better understand macrophages in fracture healing and assess its drug targetability.

Acknowledgments

The authors wish to thank Jeff Fox for assistance with the histology, and Lindsay Schnur for help with the micro-CT scans and analyses. This work was funded by research grants from AOTruama and the National Institutes of Health P30 AR069655

Part of this work was supported by the AOTrauma Clinical Priority Program, and the National Institutes of Health (P30 AR069655).

References

1. Roberts JL, Drissi H. 2020. Advances and Promises of Nutritional Influences on Natural Bone Repair. J Orthop Res 38:695–707. [PubMed: 31729041]
2. Einhorn TA, Gerstenfeld LC. 2015. Fracture healing: mechanisms and interventions. Nat Rev Rheumatol 11:45–54. [PubMed: 25266456]
3. Bahney CS, Zondervan RL, Allison P, et al. 2019. Cellular biology of fracture healing. J Orthop Res 37:35–50. [PubMed: 30370699]
4. Raggatt LJ, Wullschleger ME, Alexander KA, et al. 2014. Fracture healing via periosteal callus formation requires macrophages for both initiation and progression of early endochondral ossification. Am J Pathol 184:3192–3204. [PubMed: 25285719]
5. Vi L, Baht GS, Whetstone H, et al. 2015. Macrophages promote osteoblastic differentiation in-vivo: implications in fracture repair and bone homeostasis. J Bone Miner Res 30:1090–1102. [PubMed: 25487241]

6. Italiani P, Boraschi D. 2014. From Monocytes to M1/M2 Macrophages: Phenotypical vs. Functional Differentiation. Front Immunol 5:514. [PubMed: 25368618]
7. Schlundt C, El Khassawna T, Serra A, et al. 2018. Macrophages in bone fracture healing: Their essential role in endochondral ossification. Bone 106:78–89. [PubMed: 26529389]
8. Hozain S, Cottrell J. 2020. CDllb+ targeted depletion of macrophages negatively affects bone fracture healing. Bone 138:115479. [PubMed: 32535290]
9. Chen L, Cheng S, Sun K, et al. 2021. Changes in macrophage and inflammatory cytokine expressions during fracture healing in an ovariectomized mice model. BMC Musculoskelet Disord 22:494. [PubMed: 34049522]
10. Chow SKH, Cui C, Cheng KYK, et al. 2021. Acute Inflammatory Response in Osteoporotic Fracture Healing Augmented with Mechanical Stimulation is Regulated In Vivo through the p38-MAPK Pathway. Int J Mol Sci 22.
11. Niedermair T, Straub RH, Brochhausen C, et al. 2020. Impact of the Sensory and Sympathetic Nervous System on Fracture Healing in Ovariectomized Mice. Int J Mol Sci 21.
12. Du C, Xiao P, Gao S, et al. 2022. High Fluoride Ingestion Impairs Bone Fracture Healing by Attenuating M2 Macrophage Differentiation. Front Bioeng Biotechnol 10:791433. [PubMed: 35669059]
13. Chow SK, Wong CH, Cui C, et al. 2022. Modulating macrophage polarization for the enhancement of fracture healing, a systematic review. J Orthop Translat 36:83–90. [PubMed: 35979176]
14. Chow SK, Chim YN, Wang J, et al. 2019. Vibration treatment modulates macrophage polarisation and enhances early inflammatory response in oestrogen-deficient osteoporotic-fracture healing. Eur Cell Mater 38:228–245. [PubMed: 31697398]
15. Xu X, Wang R, Sun Z, et al. 2019. Trehalose enhances bone fracture healing in a rat sleep deprivation model. Ann Transl Med 7:297. [PubMed: 31475167]
16. Zhou W, Lin Z, Xiong Y, et al. 2021. Dual-Targeted Nanoplatform Regulating the Bone Immune Microenvironment Enhances Fracture Healing. ACS Appl Mater Interfaces 13:56944–56960. [PubMed: 34797653]
17. Zhang R, Liang Y, Wei S. 2018. M2 macrophages are closely associated with accelerated clavicle fracture healing in patients with traumatic brain injury: a retrospective cohort study. J Orthop Surg Res 13:213. [PubMed: 30157885]
18. Onofre G, Kolackova M, Jankovicova K, et al. 2009. Scavenger receptor CD163 and its biological functions. Acta Medica (Hradec Kralove) 52:57–61. [PubMed: 19777868]
19. Fujiwara Y, Ohnishi K, Horlad H, et al. 2020. CD163 deficiency facilitates lipopolysaccharide-induced inflammatory responses and endotoxin shock in mice. Clin Transl Immunology 9:e1162. [PubMed: 33005412]
20. Nishitani K, Ishikawa M, Morita Y, et al. 2020. IsdB antibody-mediated sepsis following S. aureus surgical site infection. JCI Insight 5.
21. Xie C, Liang B, Xue M, et al. 2009. Rescue of impaired fracture healing in COX-2−/− mice via activation of prostaglandin E2 receptor subtype 4. Am J Pathol 175:772–785. [PubMed: 19628768]
22. Bonnarens F, Einhorn TA. 1984. Production of a standard closed fracture in laboratory animal bone. J Orthop Res 2:97–101. [PubMed: 6491805]
23. Zhang X, Schwarz EM, Young DA, et al. 2002. Cyclooxygenase-2 regulates mesenchymal cell differentiation into the osteoblast lineage and is critically involved in bone repair. J Clin Invest 109:1405–1415. [PubMed: 12045254]
24. Yukata K, Xie C, Li TF, et al. 2018. Teriparatide (human PTH1-34) compensates for impaired fracture healing in COX-2 deficient mice. Bone 110:150–159. [PubMed: 29408411]
25. Duvall CL, Robert Taylor W, Weiss D, et al. 2004. Quantitative microcomputed tomography analysis of collateral vessel development after ischemic injury. Am J Physiol Heart Circ Physiol 287:H302–310. [PubMed: 15016633]
26. Duvall CL, Taylor WR, Weiss D, et al. 2007. Impaired angiogenesis, early callus formation, and late stage remodeling in fracture healing of osteopontin-deficient mice. J Bone Miner Res 22:286–297. [PubMed: 17087627]

27. Zhang X, Xie C, Lin A, et al. 2005. Periosteal Progenitor Cell Fate in Segmental Cortical Bone Graft Transplantations: Implications for Functional Tissue Engineering. Journal of Bone & Mineral Research In press.
28. Hildebrand T, Ruegsegger P. 1997. Quantification of Bone Microarchitecture with the Structure Model Index. Comput Methods Biomech Biomed Engin 1:15–23. [PubMed: 11264794]
29. Hildebrand T, Laib A, Muller R, et al. 1999. Direct three-dimensional morphometric analysis of human cancellous bone: microstructural data from spine, femur, iliac crest, and calcaneus. J Bone Miner Res 14:1167–1174. [PubMed: 10404017]
30. Zura R, Xiong Z, Einhorn T, et al. 2016. Epidemiology of Fracture Nonunion in 18 Human Bones. JAMA Surg 151:e162775. [PubMed: 27603155]
31. Brinker MR, Hanus BD, Sen M, et al. 2013. The devastating effects of tibial nonunion on health-related quality of life. J Bone Joint Surg Am 95:2170–2176. [PubMed: 24352770]
32. Kostenuik P, Mirza FM. 2017. Fracture healing physiology and the quest for therapies for delayed healing and nonunion. J Orthop Res 35:213–223. [PubMed: 27743449]
33. Al Farii H, Farahdel L, Frazer A, et al. 2021. The effect of NSAIDs on postfracture bone healing: a meta-analysis of randomized controlled trials. OTA Int 4:e092. [PubMed: 34746650]
34. Eastman K, Gerlach M, Piec I, et al. 2021. Effectiveness of parathyroid hormone (PTH) analogues on fracture healing: a meta-analysis. Osteoporos Int 32:1531–1546. [PubMed: 33559713]
35. Wynn TA, Vannella KM. 2016. Macrophages in Tissue Repair, Regeneration, and Fibrosis. Immunity 44:450–462. [PubMed: 26982353]
36. Clark D, Nakamura M, Miclau T, et al. 2017. Effects of Aging on Fracture Healing. Curr Osteoporos Rep 15:601–608. [PubMed: 29143915]
37. Wagner DR, Karnik S, Gunderson ZJ, et al. 2019. Dysfunctional stem and progenitor cells impair fracture healing with age. World J Stem Cells 11:281–296. [PubMed: 31293713]
38. Abdelmagid SM, Barbe MF, Safadi FF. 2015. Role of inflammation in the aging bones. Life Sci 123:25–34. [PubMed: 25510309]
39. Schmidt-Bleek K, Petersen A, Dienelt A, et al. 2014. Initiation and early control of tissue regeneration - bone healing as a model system for tissue regeneration. Expert Opin Biol Ther 14:247–259. [PubMed: 24397854]
40. Jin S, Meng C, He Y, et al. 2020. Curcumin prevents osteocyte apoptosis by inhibiting M1-type macrophage polarization in mice model of glucocorticoid-associated osteonecrosis of the femoral head. J Orthop Res 38:2020–2030. [PubMed: 32009245]
41. Lu LY, Loi F, Nathan K, et al. 2017. Pro-inflammatory M1 macrophages promote Osteogenesis by mesenchymal stem cells via the COX-2-prostaglandin E2 pathway. J Orthop Res 35:2378–2385. [PubMed: 28248001]
42. Hirosawa N, Uchida K, Kuniyoshi K, et al. 2018. Vein wrapping promotes M2 macrophage polarization in a rat chronic constriction injury model. J Orthop Res.
43. Li XC, Luo SJ, Fan W, et al. 2022. M2 macrophage-conditioned medium inhibits intervertebral disc degeneration in a tumor necrosis factor-alpha-rich environment. J Orthop Res 40:2488–2501. [PubMed: 35170802]
44. Margulies BS, DeBoyace SD, Parsons AM, et al. 2015. Functionally deficient mesenchymal stem cells reside in the bone marrow niche with M2-macrophages and amyloid-beta protein adjacent to loose total joint implants. J Orthop Res 33:615–624. [PubMed: 25418884]
45. Sunwoo JY, Eliasberg CD, Carballo CB, et al. 2020. The role of the macrophage in tendinopathy and tendon healing. J Orthop Res 38:1666–1675. [PubMed: 32190920]
46. Kawakubo A, Uchida K, Miyagi M, et al. 2020. Investigation of resident and recruited macrophages following disc injury in mice. J Orthop Res 38:1703–1709. [PubMed: 31965590]
47. Rahman K, Vengrenyuk Y, Ramsey SA, et al. 2017. Inflammatory Ly6Chi monocytes and their conversion to M2 macrophages drive atherosclerosis regression. J Clin Invest 127:2904–2915. [PubMed: 28650342]
48. Soldano S, Pizzorni C, Paolino S, et al. 2016. Alternatively Activated (M2) Macrophage Phenotype Is Inducible by Endothelin-1 in Cultured Human Macrophages. PLoS One 11:e0166433. [PubMed: 27846260]

49. Abraham NG, Drummond G. 2006. CD163-Mediated hemoglobin-heme uptake activates macrophage HO-1, providing an antiinflammatory function. Circ Res 99:911–914. [PubMed: 17068296]

50. Stilund M, Reuschlein AK, Christensen T, et al. 2014. Soluble CD163 as a marker of macrophage activity in newly diagnosed patients with multiple sclerosis. PLoS One 9:e98588. [PubMed: 24886843]

51. Reynolds DG, Takahata M, Lerner AL, et al. 2010. Teriparatide therapy enhances devitalized femoral allograft osseointegration and biomechanics in a murine model. Bone 48:562–570. [PubMed: 20950720]

52. Antebi B, Zhang L, Sheyn D, et al. 2016. Controlling Arteriogenesis and Mast Cells Are Central to Bioengineering Solutions for Critical Bone Defect Repair Using Allografts. Bioengineering (Basel) 3.

53. Zhang L, Wang T, Chang M, et al. 2017. Teriparatide Treatment Improves Bone Defect Healing Via Anabolic Effects on New Bone Formation and Non-Anabolic Effects on Inhibition of Mast Cells in a Murine Cranial Window Model. J Bone Miner Res 32:1870–1883. [PubMed: 28556967]

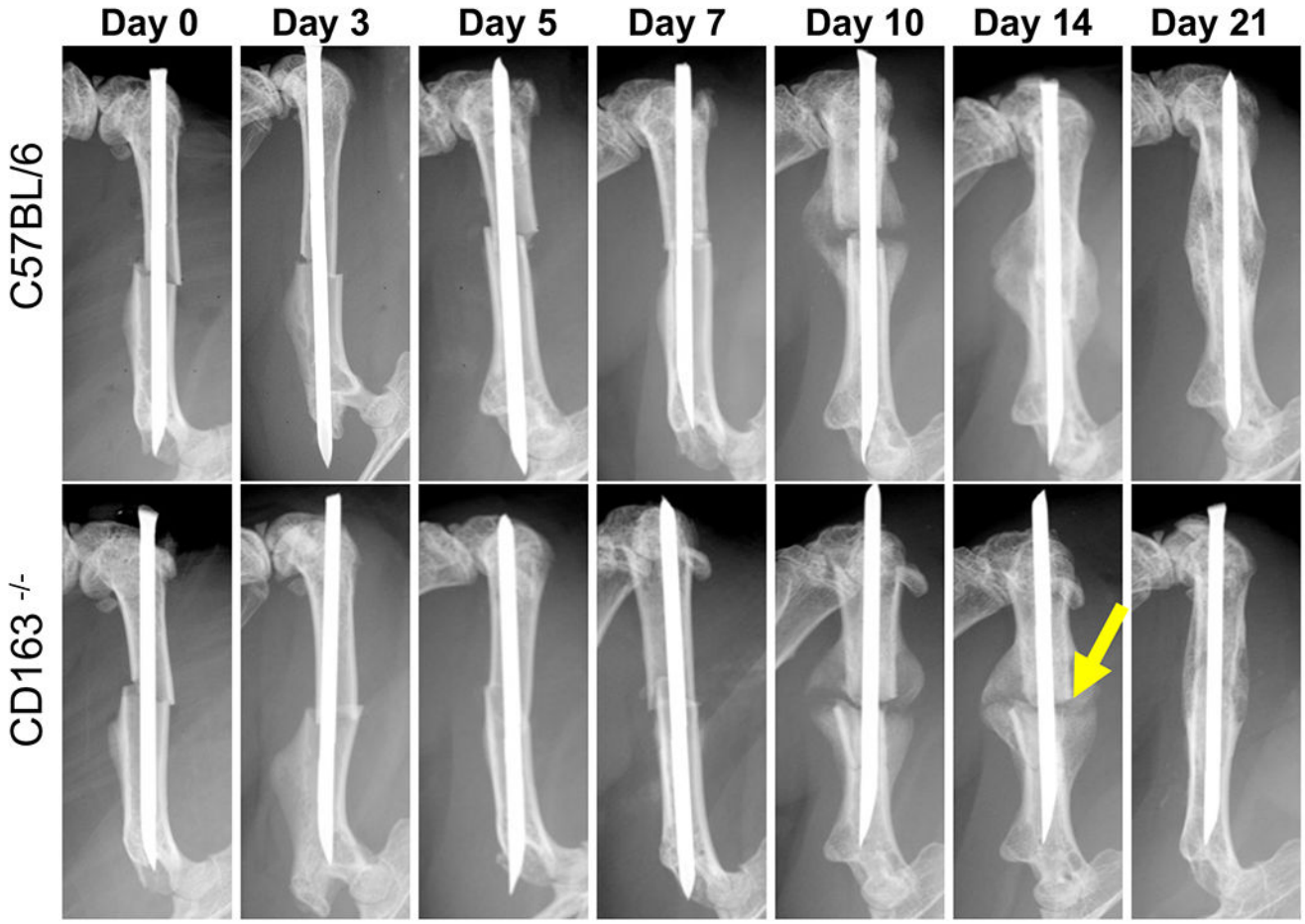

Figure 1. Radiographic evidence of delayed fracture healing in CD163$^{-/-}$ mice.

C57BL/6 and CD163$^{-/-}$ mice (n = 10, or >10) underwent mid-diaphyseal femur fracture surgery with intramedullary pin fixation. Longitudinal X-rays were obtained to assess radiographic healing. Longitudinal X-rays of fracture healing in representative C57BL/6 and CD163$^{-/-}$ mice are shown to illustrate the persistent fracture gap (yellow arrow) in the mutant mice on day 14 post-surgery.

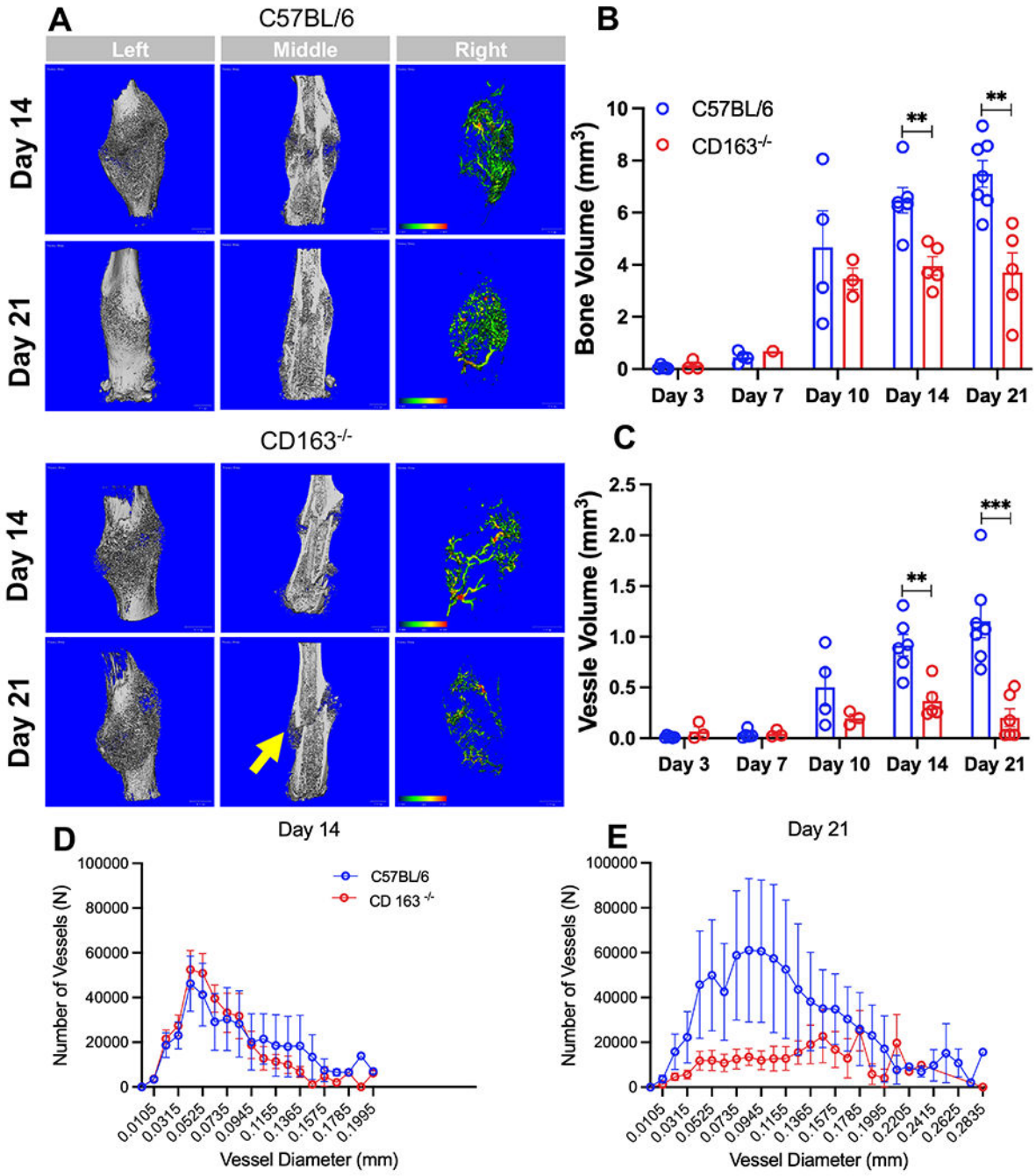

Figure 2. Vascular micro-CT evidence of delayed fracture healing in CD163$^{-/-}$ mice.

C57BL/6 and CD163$^{-/-}$ mice (n≥3) received femur fracture as described in Figure 1, they were euthanized via Microfil perfusion on day 14 or 21, post-surgery and the fractured femurs were processed for vascular micro-CT. (A) 3D renderings of representative femurs (left), with saggital view (middle) and perfused vasculature (right) are shown to illustrate the apparent delayed union (arrow), decreased fracture callus and poor vascularization in CD163$^{-/-}$ mice. (B) Quantitative analyses revealed that compared with C57BL/6 control, bone volume in CD163$^{-/-}$ fractures was reduced 74%, 61% ($p<0.01$), and 49% ($p<0.01$) (*t*

test) ; and (C) the vasculature was reduced to 40%(**$p<0.01$) and 18% (***$p<0.001$), on days 10, 14, and 21 post-fracture, respectively. (D) On day 14, the vessel diameter, which around the fracture site was not significantly different between C57BL/6 and CD163$^{-/-}$ mice, m ranged from Φ 0.0105 to Φ 0.1995 mm. On day 21(E), there was formation of much thicker vessels (Φ > 0.1995 mm). Besides, the f vessels with a diameter range from Φ 0.0105 to Φ 0.1995 mm were more abundant in C57BL/6 than CD163$^{-/-}$ mice.

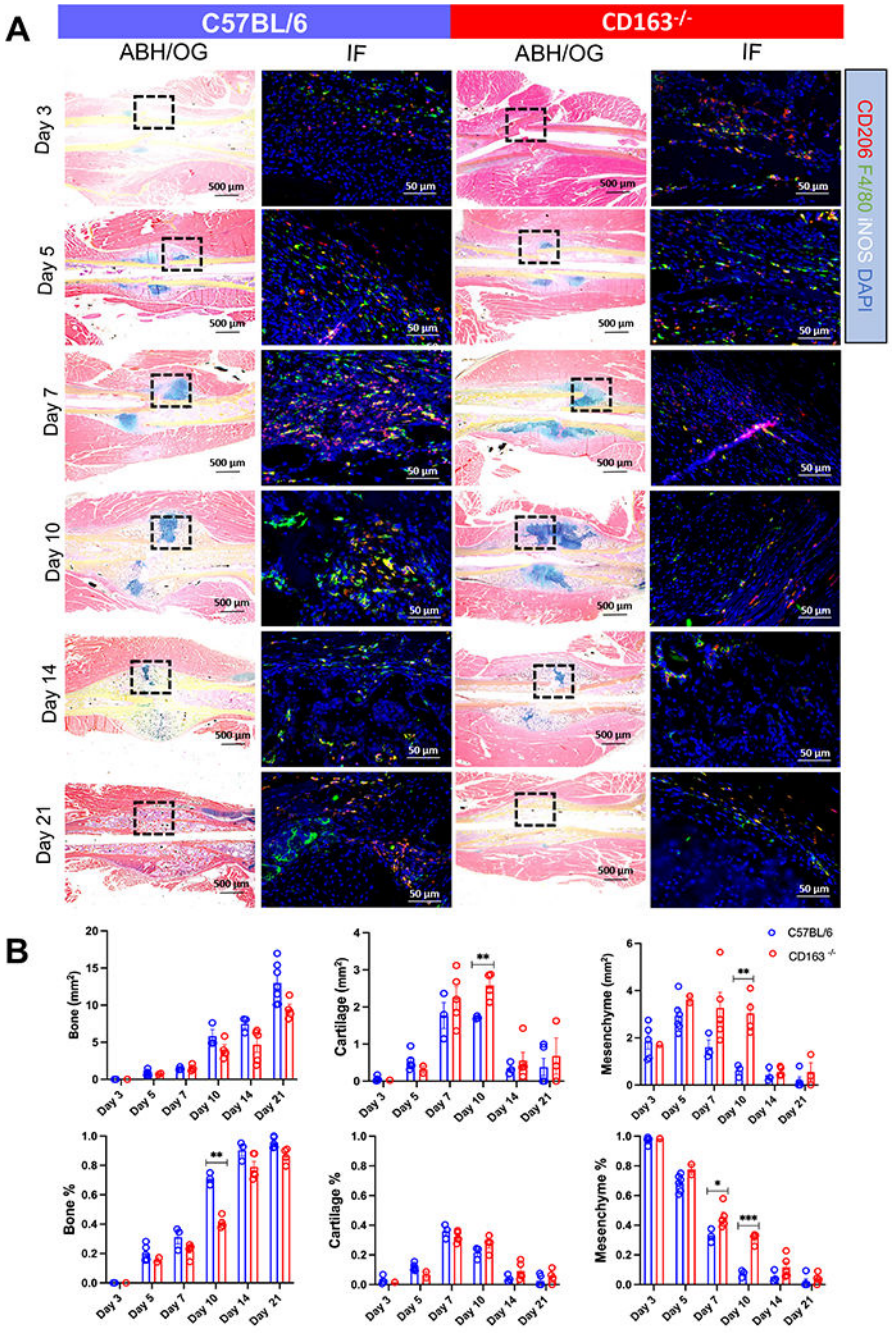

Figure 3. Histologic evidence of delayed fracture healing and impaired macrophage infiltration in CD163$^{-/-}$ mice.

C57BL/6 and CD163$^{-/-}$ mice (n≥3) received femur fracture as described in Figure 1. Fractured femurs were harvested on the indicated day and processed for OG/AB-stained histology and immunofluorescence (*IF*). (A) Representative OG/AB-stained histology is shown at 10x, highlighting the large amount of persistent Alcian blue stained cartilage in CD163$^{-/-}$ vs. C57BL/6 fracture callus on day 7 & 10 post-fracture. Representative IF images are shown at 20x. Note the presence of F4/80^{+} macrophages (green) in C57BL/6 fractures throughout healing, and their scarcity in CD163$^{-/-}$ fractures. (B)

Visiopharm histomorphometry was performed to quantify the amount of bone, cartilage and undifferentiated mesenchyme tissue in the fractured femurs. Data from each mouse is graphed as the mean for the group +/− SD (*t* test, *p<0.05, **p<0.01, ***p<0.001).

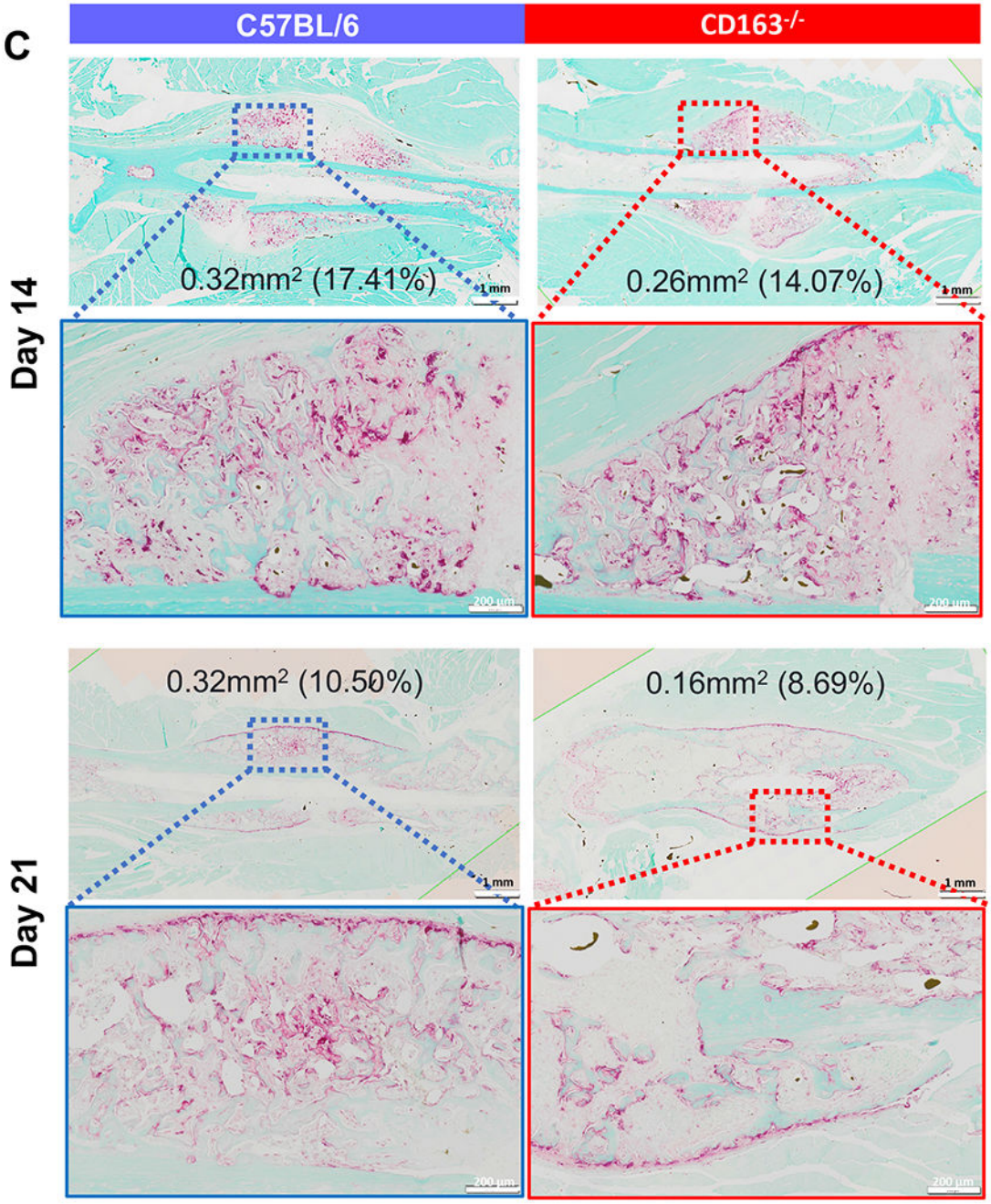

Figure 4. Normal osteoclastogenesis in CD163$^{-/-}$ fracture callus.

Bone sections from C57BL/6 and CD163$^{-/-}$ mice (day 14 and day 21 fractures) described in Figure 3 were stained with tartrate-resistant acid phosphatase (TRAP). Representative 20x images with magnified region of interest (box, 5x magnification) are shown. The TRAP^{+} area and percentage of the fracture callus were quantified using Visiopharm Histomorphometry software. No remarkable differences were found in the osteoclasts surrounding the C57BL/6 and CD163$^{-/-}$ fractures at these time points.

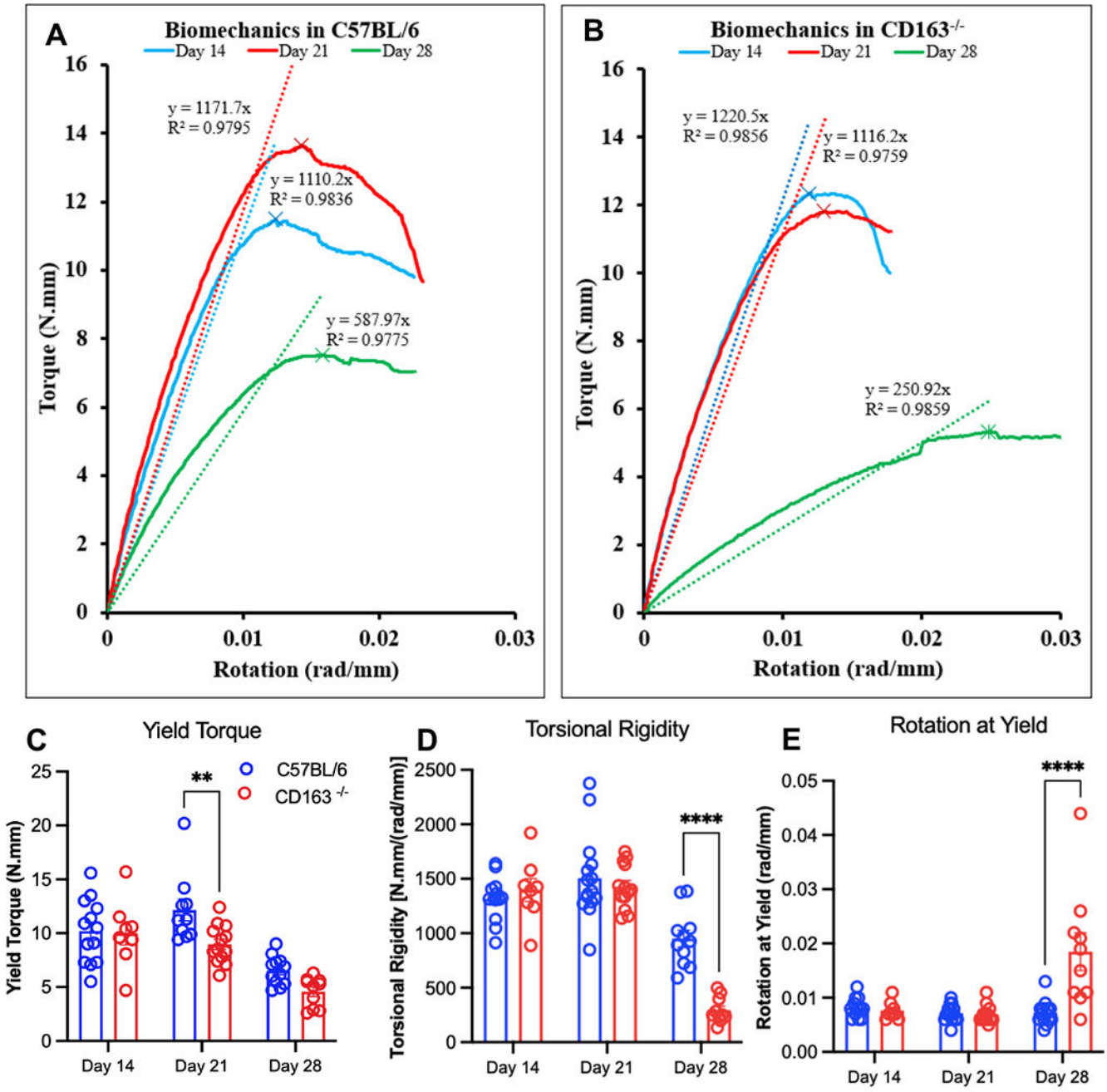

Figure 5. Defective biomechanical fracture healing in CD163$^{-/-}$ mice.

C57BL/6 and CD163$^{-/-}$ mice (n≥5) received femur fracture as described in Figure 1, and the fractured femurs were harvested on 14, 21 or 28 and processed for torsion testing to failure. Primary data from representative femurs are shown with the data for each mouse +/− SD for the group (2-way ANOVA,*p<0.05).